Analysis of a low-finesse Fabry–Perot sensing interferometer illuminated by a multimode optical fiber

Frédéric Pérennès, Paul C. Beard, and Tim N. Mills

A model of the reflected fringe system for an ideal plane-parallel, low-finesse Fabry–Perot (FP) cavity illuminated by a multimode optical fiber has been developed and experimentally validated. This showed that the phase dispersion within the cavity arising from the divergent nature of the incident illumination significantly degrades the visibility of the reflected fringes. Departures from the ideal FP cavity are also examined. The effect on fringe visibility when the plane of the FP cavity is tilted with respect to the fiber axis and when the cavity surfaces are no longer perfectly parallel to each other has been explored. The analysis described is relevant to the design and the optimization of multimode optical-fiber sensors that use FP sensing cavities. © 1999 Optical Society of America

OCIS codes: 060.2370, 120.2230.

1. Introduction

Extrinsic Fabry–Perot (FP) interferometer (EFPI) optical-fiber sensors have been reported in the literature for their high sensitivity to temperature, strain, vibration and acoustic waves.[1,2] Many of these EFPI sensors use a single-mode fiber in association with a FP interferometer (FPI) fabricated when a reflector is placed at a distance (typically less than a few hundred micrometers) from the fiber end face. The reflections at the fiber–air boundary and at the reflector interfere, and the light reflected back into the fiber is modulated when the thickness of the cavity is changed by one of the above parameters. For an intensity-based low-finesse FPI sensor, the sensitivity to a measurand-induced change in cavity thickness is proportional to the visibility of the interference fringes reflected back into the fiber. The fringe visibility of a low-finesse cavity illuminated by a single-mode optical fiber can be analyzed by modeling of the output of the fiber as a point source[3] or, more accurately, as a Gaussian beam.[4] These analyses show that the aperturing effect of the fiber (because of its small core diameter of a few micrometers) reduces the effective reflection coefficient of the second surface of the cavity and is the dominant mechanism for degrading fringe visibility.

In this paper we are interested in an EFPI illuminated by a multimode optical fiber. Such a configuration has been previously explored with thin polymer films as FP sensing interferometers for the detection of acoustic and thermal signals.[5–9] Multimode EFPI sensors have also been investigated for strain measurement in engineering materials.[10]

The analyses used to model single-mode EFPI's[3,4,11] are no longer applicable, as the output of a multimode optical fiber approximates that of an extended source rather than a point source or a Gaussian beam. Additionally, the relatively large core diameters of multimode fibers mean that the aperturing effect of the fiber is generally of much less significance. As we describe in this paper, it is the effect of phase dispersion within the interferometer caused by the divergence of the incident illumination and nonuniformities in cavity thickness that are mainly responsible for limiting fringe visibility when a multimode optical fiber is used. This is in contrast to single-mode EFPI's, in which phase-dispersion effects tend to be small because of the small area of the illuminated region.

We present a theoretical description of the transfer function and visibility of an ideal plane-parallel FPI illuminated by a multimode optical fiber in Section 2. This model is validated experimentally in Section 3 and used as a basis for studying departures from the ideal FPI in Section 4. Two typical imperfections

The authors are with the Department of Medical Physics and Bioengineering, University College London, Shropshire House, 11-20 Capper Street, London WC1E 6JA, United Kingdom. F. Pérennès (perennesf@elettra.trieste.it) permanent address is Sincrotrone Trieste, Experimental Division in Area Science Park, S.S. 14 Km 163, 5, 34012 Basovizza, Trieste, Italy.

Received 19 April 1999; revised manuscript received 6 August 1999.

0003-6935/99/347026-09$15.00/0

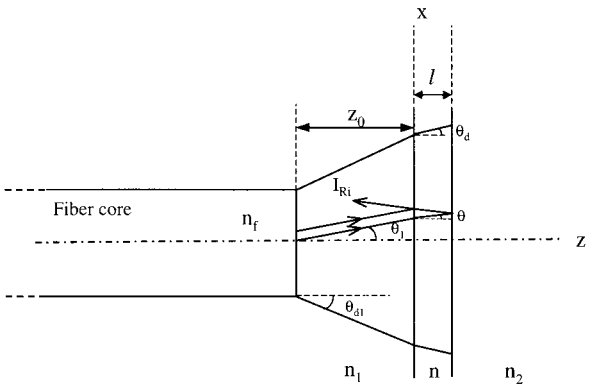

Fig. 1. Schematic of a plane-parallel low-finesse FPI illuminated by a multimode optical fiber. θ_{d1} and θ_d are the angles of the most diverging rays in the media between the fiber and the FPI and in the FP cavity, respectively. θ_1 and θ are the angles of a particular ray in the media between the fiber and the FPI and in the FP cavity, respectively.

are studied. First we consider the case in which the FPI is not perfectly perpendicular to the fiber axis. Second, we consider the case in which the cavity surfaces are not perfectly parallel to each other, resulting in variations in cavity thickness over the illuminated region.

2. Transfer Function of an Ideal Low-Finesse Fabry–Perot Interferometer Illuminated by a Multimode Fiber

In this section we derive the relationship between the reflected intensity output and the phase difference for an ideal low-finesse FPI illuminated by a multimode optical fiber. This relationship, termed the transfer function, is then used to obtain the visibility of the reflected fringes.

A schematic of a FPI, illuminated by the output of a multimode optical fiber, is shown in Fig. 1. In practice, such a FP cavity could be formed either by a solid plane-parallel transparent plate (e.g., glass or a polymer) or an air gap between two parallel optical flats perpendicular to the fiber axis. The FPI is located at a distance z_0 from the fiber end face. The medium between the fiber and the FPI has a refractive index n_1, and the medium on the external side of the FPI has a refractive index n_2. The refractive index inside the FPI is n, and n_f is the refractive index of the fiber core. The reflection coefficients of the mirrors of the interferometer are defined by the weak Fresnel reflections arising from the refractive-index mismatches at the two surfaces of the interferometer and are therefore small.

It is assumed that all the propagation modes in the optical fiber are equally excited. Thus the output light distribution at the distal end of the fiber is of uniform intensity and conforms to that of a top-hat profile. Under these conditions, the maximum angle of divergence θ_m depends on the numerical aperture (NA) of the fiber and, in air, is given by $\theta_m = \arcsin(\mathrm{NA})$. The light emerging from the fiber can be represented by the sum of wave fronts of equal amplitude, leaving the fiber at different angles distributed between 0 and θ_{d1}. Angles θ_{d1} and θ_d are the angles of the most diverging wave fronts in the medium between the fiber and the FPI and inside the FPI, respectively. They obey Snell's law:

$$\sin \theta_{d1} = \frac{n}{n_1} \sin \theta_d. \tag{1}$$

Two parallel incident rays, corresponding to an internal angle θ within the FPI, are reflected on both sides of the cavity and interfere, as shown in Fig. 1. Because of the low spatial coherence of the output of a multimode fiber (which is due to the different phases of individual modes), it is necessary that both the FPI thickness and the maximum angle of divergence be be small. This ensures that the two interfering rays originate from nearly the same point on the optical-fiber end face and are therefore located within a region of spatial coherence and are correlated in phase. Under these conditions, uncorrelated random variations in the absolute phase across the fiber output that are due to external perturbations of the fiber do not affect the interference process. The net phase difference between the two reflections is given by[12]

$$\phi(\theta) = \frac{4\pi n l}{\lambda} \cos \theta, \tag{2}$$

where n is the refractive index in the FP cavity, l is the cavity thickness, and λ is the light-source wavelength. The weak Fresnel reflections at the interferometer surfaces allow us to neglect the effect of multiple reflections inside the cavity.[13] Thus the cavity acts as a low-finesse FPI, and the intensity of the reflected light is simply due to the coherent superposition of the two Fresnel reflections. The reflected intensity resulting from the interference of two parallel rays for an internal angle θ is given by

$$I_{R_i}(\theta) = \frac{I_0}{\Delta\phi}[R_1 + (1 - R_1)^2 R_2 + 2(R_1 R_2)^{1/2} \times (1 - R_1)\cos \phi(\theta)], \tag{3}$$

where I_0 is the total intensity of the light incident upon the FPI. R_1 and R_2 are the Fresnel reflection coefficients on each side of the interferometer. $\Delta\phi$ is the total phase dispersion and is a measure of the range of optical path lengths taken by interfering rays at different angles θ within the interferometer, as discussed below. When observed in a plane perpendicular to the fiber axis, the reflected light forms a pattern of concentric circular fringes of equal inclination. Dark fringes correspond to the interference of rays propagating at an angle of $\theta = \arccos\{[(2m + 1)\lambda]/4nl\}$ inside the FP cavity and bright fringes to rays propagating at an angle $\theta = \arccos(2m\lambda/4nl)$, where m is an integer. The maximum phase difference occurs for a ray propagating along the fiber axis with $\theta = 0$, and the minimum phase difference occurs for the most divergent ray $\theta = \theta_d$ in the cavity. Thus the effect of divergence is to introduce dispersion into

the phase difference. This phase dispersion can be expressed as

$$\Delta\phi = \phi_{\max} - \phi_{\min} = \frac{4\pi n l}{\lambda}(1 - \cos\theta_d) = \phi_0(1 - \cos\theta_d), \quad (4)$$

where ϕ_0 is the phase difference for a normally incident beam. The top-hat incident intensity profile yields a uniform distribution of phase difference in the interval defined by

$$\begin{cases} D(\phi) = 1 & \text{for } \phi_0 - \Delta\phi < \phi < \phi_0 \\ D(\phi) = 0 & \text{elsewhere} \end{cases}. \quad (5)$$

To calculate the total reflected light I_R it is necessary to integrate the expression in Eq. (3) over the range of phase dispersion introduced by the divergence of light at the fiber output:

$$I_R = \int_{\Delta\phi} D(\phi) I_{R_i}(\phi)\mathrm{d}\phi = \left[R_1 + (1 - R_1)^2 R_2 + \frac{2(R_1 R_2)^{1/2}(1 - R_1)}{\Delta\phi} \int_{\phi_0 - \Delta\phi}^{\phi_0} \cos\phi \mathrm{d}\phi \right] I_0. \quad (6)$$

This expression can be evaluated analytically and gives

$$I_R = \left[R_1 + (1 - R_1)^2 R_2 + 2(R_1 R_2)^{1/2}(1 - R_1) \times \frac{\sin(\Delta\phi/2)}{\Delta\phi/2} \cos\left(\phi_0 - \frac{\Delta\phi}{2}\right) \right] I_0, \quad (7)$$

where I_0 is the total incident light intensity in the FP plane. From Eq. (7) the maximum and the minimum values of the reflected intensity, $I_{\max}$ and $I_{\min}$, occur when $\phi_0 - \Delta\phi/2 = 2k\pi$ and $\phi_0 - \Delta\phi/2 = (2k + 1)\pi$, respectively, where k is an integer. The analytical solution for the fringe visibility $(I_{\max} - I_{\min})/(I_{\max} + I_{\min})$ is simply expressed as

$$\gamma = \frac{2(R_1 R_2)^{1/2}(1 - R_1)}{R_1 + (1 - R_1)^2 R_2} \frac{|\sin\Delta\phi/2|}{\Delta\phi/2} = \gamma_0 \frac{|\sin\Delta\phi/2|}{\Delta\phi/2}, \quad (8)$$

where γ_0 is the visibility for a collimated incident beam. γ is zero for $\Delta\phi = 2k\pi$ (k is an integer).

Equation (8) describes the visibility of the fringes reflected from the interferometer before they enter the optical fiber. We have already made the assumption that the cavity thickness and the internal divergence are sufficiently small that near-complete overlap occurs between the reflections on the two sides of the cavity—reasonable for cavities a few hundred micrometers thick illuminated with output of a typical multimode optical fiber of NA ~ 0.2. If we are to use Eq. (8) to model the visibility of the fringes that would be observed at the other end of the fiber, we now need to make the additional assumptions that z_0 is small and that the fiber core diameter is sufficiently large that the degradation in visibility arising from the modification of R_1 and R_2 that is due to the aperturing effect of the fiber is small. These assumptions are reasonable, given the relatively large core diameters of multimode optical fibers and that in most practical multimode EFPI configurations the cavity is situated close to or in contact with the fiber end.

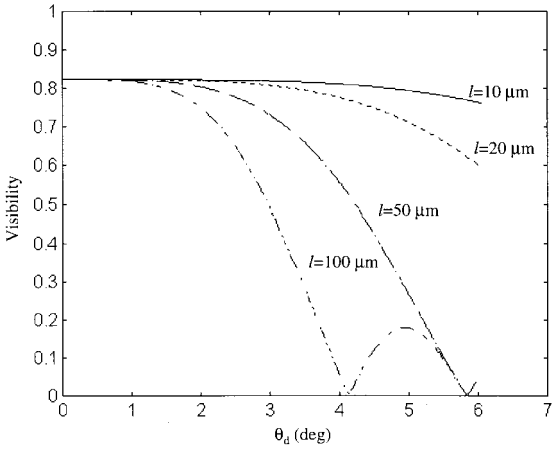

Fig. 2. Visibility versus maximum internal beam divergence θ_d for different values of the cavity thickness l, $z_0 = 0$, $n = 1.64$, $n_1 = n_f = 1.47$, $n_2 = 1.33$, and $\lambda = 850$ nm.

Equation (8) is now used to model the visibility of a low-finesse FP cavity for a range of divergence angles and cavity thicknesses. The case in which a solid FPI is placed in optical contact with the tip of a multimode optical fiber is considered (i.e., $z_0 = 0$). Such a configuration represents a physically useful case. It could, for example, be used to realize a sensing probe of the type described in Ref. 9, in which a transparent polymer film acts as an acoustically and thermally sensitive FP cavity. We consider the particular case in which a FP cavity of refractive index $n = 1.64$ is in optical contact with the end of the fiber ($n_1 = n_f = 1.47$) and immersed in water ($n_2 = 1.33$).

Figure 2 shows the visibility versus the maximum beam divergence angle θ_d inside the FPI for typical values of the cavity thickness. These curves can be used to predict the maximum theoretical value of the visibility for a given FPI thickness and divergence. Note that for all cavity thicknesses the maximum visibility is 0.83 rather than 1 because the Fresnel reflection coefficients, because of the refractive-index mismatches on the two sides of the FPI in this configuration, are not the same. The analysis of Fig. 2 reveals that the phase dispersion that is due to an internal divergence of more than a couple of degrees begins to significantly degrade visibility for cavity thicknesses as small as even 50 μm. This means that low-NA fibers must be used to maintain the visibility of a FPI multimode fiber sensor close to its maximum.

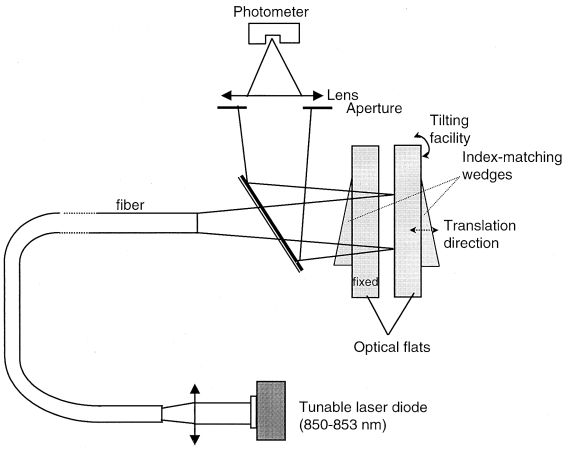

Fig. 3. Experimental setup for the validation of FP transfer function and visibility, $R_1 = R_2 = 0.04$, $\theta_d = 3.7°$, $z_0 = 22$ cm, step-index fiber with 380-μm core diameter and NA = 0.12, $n = n_1 = n_2 = 1$.

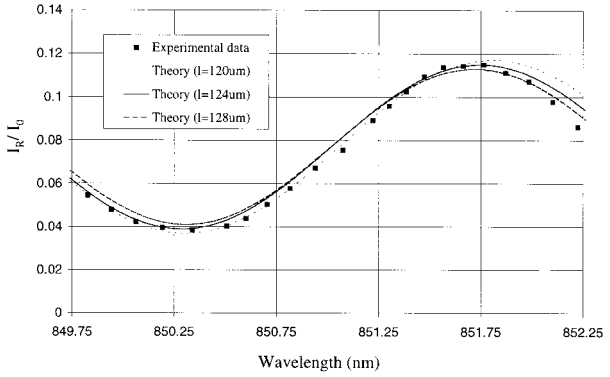

Fig. 4. Transfer function of FP obtained by wavelength tuning.

3. Experimental Validation of the Transfer Function

To validate the expression calculated in Eq. (8) it is necessary to measure the fringe visibility as a function of phase dispersion. We achieved this by varying the separation of two optical flats that formed a FP cavity and by measuring visibility as a function of thickness for a fixed θ_d.

The experimental setup is shown in Fig. 3. Light from a tunable laser diode (850–853 nm) is launched into a multimode fiber (380-μm core diameter, NA = 0.12) that is bent several times along its 10-m length in order to excite all the propagation modes so as to produce a divergent beam with a quasi-top-hat intensity profile at the distal end of the fiber. Two optical flats facing each other are placed in the path of the light beam perpendicular to the fiber axis. The air gap between the flats creates a FPI whose thickness can be changed by adjusting the position of the right-hand flat, which is mounted on a translation stage, with a 20-μm step graduated vernier. To avoid the parasitic reflections from the front and the back faces of the optical flats, angled cover slips were attached with index-matching gel, as shown in Fig. 3.

A beam splitter is inserted between the fiber and the FPI to deflect the reflected light onto an aperture. The light traveling through the aperture is collected by a lens and focused onto a photodetector. The measured intensity is thus equivalent to the intensity of the light that would be reflected back into the fiber if the FP cavity were close to the fiber. We obtain the parallelism between the two flats by ensuring that the observed fringe pattern in a plane perpendicular to the optical path is a succession of concentric bright and dark centered rings. The diameter D of the aperture limits the maximum divergence of the beam to an angle $\theta_d = \arctan[(D/2)/z]$, where z is the optical path length of the light between the fiber tip and the aperture plane. D is set in order to have $\theta_d < \theta_m$ so that only the light with a divergence of less than θ_d contributes to the detected intensity. The aperture therefore provides a convenient way to control the divergence. The maximum divergence was set to $\theta_d = 3.7°$, and the thickness of the cavity was tuned from 20 to 400 μm to be able to vary the phase dispersion from 0 to approximately 4π. Once the vernier is set to a particular thickness, a small change in thickness is applied to produce a π phase shift so that a maximum and a minimum can be observed to measure the visibility.

The micrometer enabled only changes in the thickness of the cavity to be made with high accuracy. To obtain absolute cavity thickness measurements, it was therefore necessary to calibrate the micrometer for a particular cavity thickness and reference all other measurements to this. We achieved the calibration by tuning the wavelength of the laser source and measuring the reflected light intensity versus the wavelength for one particular position of the vernier. When the gap $\Delta\lambda$ separating a minimum and a maximum of the reflected fringes is measured, the thickness of the cavity can be deduced from Eqs. (4) and (7):

$$l = \frac{\lambda^2}{2n(1 + \cos\theta_d)\Delta\lambda}, \tag{9}$$

where λ is the wavelength halfway between the consecutive minimum and maximum. Figure 4 shows the variation of the normalized reflected intensity as a function of wavelength obtained when the laser diode is tuned over 2.5 nm for a particular vernier setting. From the experimental data in Fig. 4 we measure $\Delta\lambda = 1.46$ nm with an error of ± 0.05 nm. The thickness for this particular position of the vernier is obtained with Eq. (9) and gives $l = 124$ μm with an error of ± 4 μm resulting from the error on the measurement of $\Delta\lambda$. Theoretical transfer functions for cavity thicknesses within the error interval (i.e., $l =$ 120, 124, and 128 μm) obtained with Eq. (7) are plotted in Fig. 4 and fit well to the experimental data.

The experimental data for the visibility as a function of phase dispersion are plotted and compared with the theory in Fig. 5. The error on the thickness calibration yields to an error of ± 0.12 rad on the phase-dispersion determination. Good agreement is found for phase dispersion below ~5 rad, and the measured visibility exhibits, as expected, a minimum

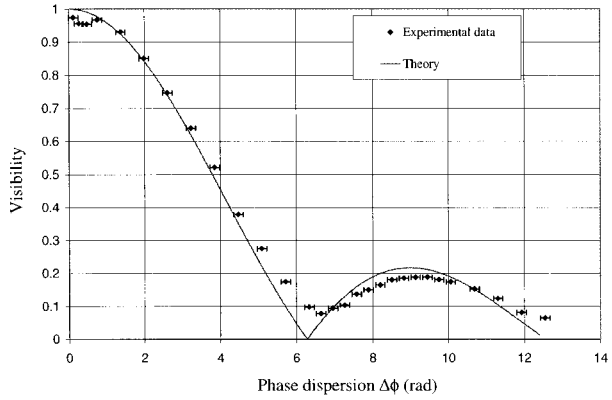

Fig. 5. Comparison between theory and experiment of visibility versus phase dispersion.

at a phase dispersion close to 2π. Note that the visibility measured at $\Delta\phi = 3.8$ rad corresponding to $l = 124$ μm is ~0.5, which also agrees with the value obtained in Fig. 4 by wavelength tuning. The fact that the experimentally measured visibility departs from theory at approximately $\Delta\phi = 2\pi$ can be attributed to experimental misalignments such as a tilt angle between the fiber axis and the plane of the interferometer or an angle between the surfaces of the interferometer. The effect of these on visibility are examined in the subsections below.

4. Departures from the Ideal Fabry–Perot Interferometer

A. Effect of a Tilt

A tilt angle between the FPI and the fiber end face breaks the radial symmetry centered on the fiber axis and changes the distribution of angles inside the FPI. The geometry for a tilt between the FPI and the fiber end face is shown in Fig. 6. The tilt angle ε_t is represented by a rotation of the fiber around the Ox axis perpendicular to the fiber axis. For mathematical convenience this rotation is centered at the origin of a light cone positioned at a distance z_i from the FP film given by the relation

$$z_i = z_0 + \frac{a}{\tan\theta_{d1}}, \tag{10}$$

where z_0 is the distance between the center of the untilted fiber end face and the FPI and a is the fiber core radius.

This new distribution of phase differences is dependent on the radial direction in the plane perpendicular to the fiber axis. The beam footprint on the front side of the FPI is no longer a disk but an ellipse centered at point O', defined by the equation

$$\frac{(x - x_0)^2}{b^2} + \frac{y^2}{c^2} = 1, \tag{11}$$

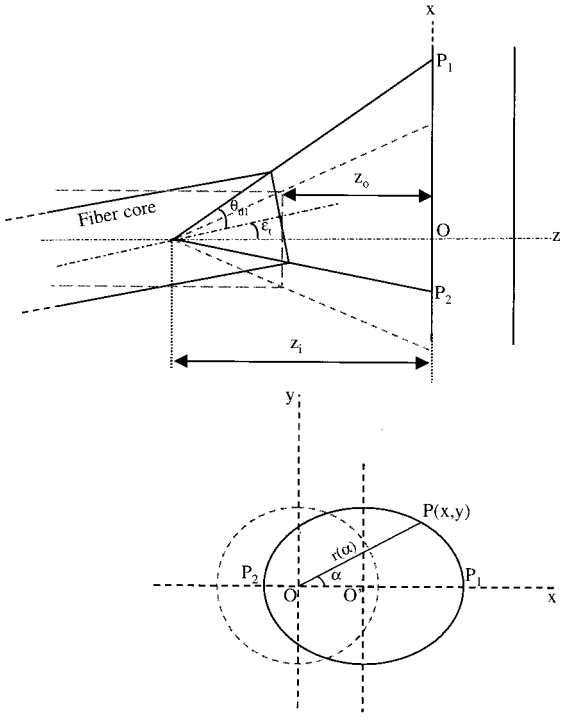

Fig. 6. Geometry describing a tilt between the fiber end face and the FPI. ε_t is the tilt angle, z_0 is the distance between the untilted fiber end face and the FPI, and z_i is the distance between the virtual origin of the light cone of angle θ_{d1} and the FPI. The ellipse centered on O' represents the beam footprint on the front side of the FPI.

with

$$x_0 = \frac{z_i}{2}[\tan(\theta_{d1} + \varepsilon_t) - \tan(\theta_{d1} - \varepsilon_t)], \tag{12}$$

$$b = \frac{z_i}{2}[\tan(\theta_{d1} + \varepsilon_t) + \tan(\theta_{d1} - \varepsilon_t)], \tag{13}$$

$$c = z_i \tan\theta_{d1}. \tag{14}$$

Equation (11) can be expressed in polar coordinates with $x = r\cos\alpha$ and $y = r\sin\alpha$, where r is the distance OP and α is the angle between the OP and the Ox axes. The radius r can be expressed versus angle α by solving second-degree equation (11), and the exact result is given by

$$r(\alpha) = \frac{x_0 c^2\cos\alpha + [c^2\cos^2\alpha + (b^2 - x_0^2)\sin^2\alpha]^{1/2}}{c^2\cos^2\alpha + b^2\sin^2\alpha}. \tag{15}$$

For optical fibers with NA's less than 0.2, the maximum angle of divergence θ_{d1} remains below 12° in air. This allows Eqs. (12) and (13), and thus Eq. (15), to be simplified as

$x_0 = z_i\tan\varepsilon_t$, $b = z_i\tan\theta_{d1}$, giving

$$r(\alpha) = z_i\tan\theta_{d1}\left\{\frac{\varepsilon_t}{\theta_{d1}}\cos\alpha + \left[1 - \left(\frac{\varepsilon_t}{\theta_{d1}}\sin\alpha\right)^2\right]^{1/2}\right\}. \tag{16}$$

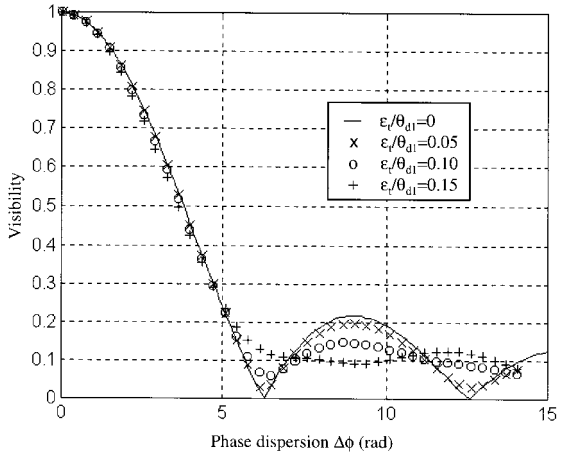

Fig. 7. Visibility versus phase dispersion for different values of the tilt angle ε_t to beam divergence θ_{d1} ratio. $R_1 = R_2 = 0.04$, $\theta_{d1} = \theta_d = 4°$, $z_0 = 22$ cm, $n = n_1 = n_2 = 1$.

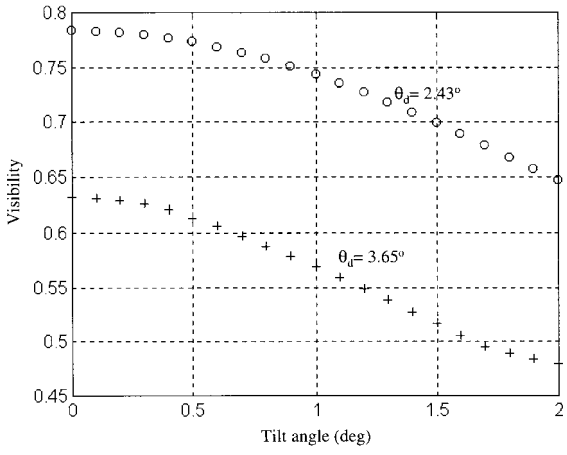

Fig. 8. Visibility versus tilt angle for a 50-μm-thick polymer cavity in optical contact with the fiber tip for two different values of the divergence θ_d ($z_0 = 0$, $n = 1.64$, $n_1 = n_f = 1.47$, $n_2 = 1.33$, $l = 50$ μm, and $\lambda = 850$ nm).

The distribution of incidence angles $\theta(\alpha)$ in the FPI can be obtained for each radial direction with

$$\theta_1(\alpha) = \arctan\frac{r(\alpha)}{z_i} = \theta_{d1}\left\{\frac{\varepsilon_t}{\theta_{d1}}\cos\alpha + \left[1 - \left(\frac{\varepsilon_t}{\theta_{d1}}\sin\alpha\right)^2\right]\right\}, \quad (17)$$

$$\theta(\alpha) = \arcsin\left(\frac{n_1}{n}\sin\theta_1(\alpha)\right). \quad (18)$$

This is an interesting result as it shows that the departure from the perfect case that is due to a tilt of the FPI along the fiber axis depends on only the ratio of the tilt angle over the divergence of the beam.

In each direction α, the distribution of phase difference is uniform between that of the most diverging beam $\theta(\alpha)$ and that of the on-axis beam ($\theta = 0$):

$$\begin{cases} D(\phi) = 1 \text{ for } \phi_0 - \Delta\phi(\alpha) < \phi < \phi_0 \\ \quad \text{with } \Delta\phi(\alpha) = \phi_0[1 - \cos\theta(\alpha)] \\ D(\phi) = 0 \text{ elsewhere} \end{cases}. \quad (19)$$

The ellipse is symmetrical around the plane $OxOz$, so the reflected light intensity can be obtained by integration over the range of angles α between 0 and π:

$$I_R = \frac{1}{\pi}\int_0^{\pi}\int_{\phi_0-\Delta\phi(\alpha)}^{\phi_0} D(\phi) I_{R_i}(\phi)\,d\phi\,d\alpha, \quad (20)$$

$$I_R = \left\{R_1 + (1-R_1)^2 R_2 + 2(R_1R_2)^{1/2}(1-R_1) \times \frac{1}{\pi}\int_0^{\pi}\frac{\sin[\Delta\phi(\alpha)/2]}{\Delta\phi(\alpha)/2}\cos\left[\phi_0 - \frac{\Delta\phi(\alpha)}{2}\right]d\alpha\right\} I_0. \quad (21)$$

The above integral is numerically evaluated and the reflected fringe visibility is then calculated for different thicknesses of the FP cavity. The visibility versus the average phase dispersion $\Delta\phi = \phi_0(1 - \cos\theta_d)$ is plotted in Fig. 7 for realistically small values of the ratio $\varepsilon_t/\theta_{d1}$. The results show that for low phase dispersion (i.e., corresponding to low FP thickness), the effect of a tilt on the fringe visibility is very small. For a FP thickness corresponding to a phase dispersion of 2π, the visibility is not zero because the fiber axis is no longer an axis of symmetry for the FPI, causing the real phase dispersion not to be equally distributed between 0 and 2π. This could be an explanation for the difference observed between the experimental result and the theory for phase dispersion close to 2π in Fig. 5.

We now examine the effect of a tilt angle on the practical configuration in which the FP cavity is in optical contact with the tip of the fiber. In this configuration, a tilt angle occurs if the fiber end face is not perfectly orthogonal to the fiber axis, perhaps because of imperfections in the polishing or cleaving of the fiber end. We consider a 50-μm-thick cavity ($n = 1.64$) directly bonded onto a 380-μm core diameter fiber tip. It is assumed that the tilt angle, cavity thickness, and beam divergence are all sufficiently small that all the light reflected by the FP polymer film cavity goes back into the fiber. We perform the calculation by using Eq. (21) but we set $z_0 = 0$, $n_1 = n_f$, $\theta_{d1} = \theta_d$, and $n_2 = 1$. The visibility versus tilt angle is calculated for θ_d equal to 2.43° and 3.65°, corresponding to fiber output divergences in air of 4° and 6°. The results are shown in Fig. 8 and indicate that a 1° tilt yields a 5% drop in visibility for $\theta_d = 2.43°$ and 16% for $\theta_d = 3.65°$. Therefore we can deduce that tilt angles should not significantly exceed 1° in order to maintain a visibility close to the maximum. Such a tolerance can readily be achieved with standard polishing or cleaving methods to prepare the end of a fiber. Note that this example is for low-NA fibers (NA < 0.1); for larger NA's, the tolerance on the fiber end angle will be correspondingly smaller.

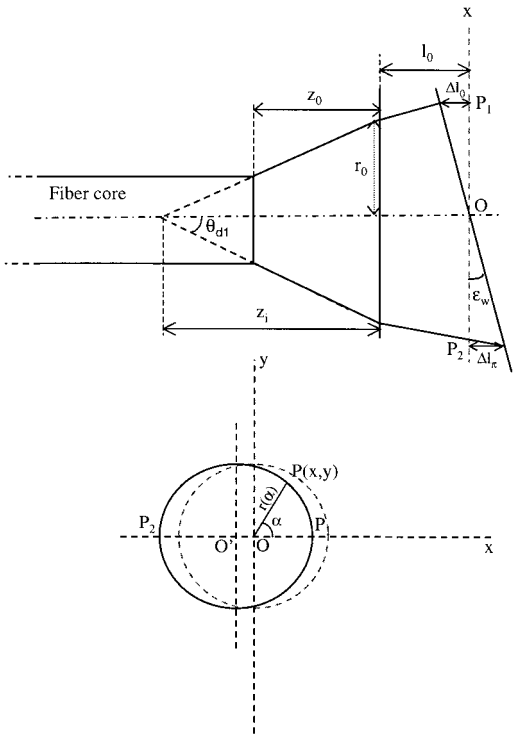

Fig. 9. Geometry showing a FP cavity with a wedge between the two surfaces. ε_w is the wedge angle, l_0 is the equivalent ideal FP cavity thickness (i.e., with no wedge), r_0 is the radius of the beam circular footprint on the front side of the FPI, and Δl_0 and Δl_π are the changes in thickness of the FP cavity for $\alpha = 0$ and $\alpha = \pi$, respectively. The ellipse centered in O' represents the projection of the beam footprint on the back side of the FPI into the $OxOy$ plane.

B. Effect of a Wedge

We now consider the case in which the two surfaces of the interferometer are not perfectly parallel to each other. The cavity geometry therefore becomes that of a wedge, introducing variations in the thickness of the interferometer across the illuminated region.

The geometry of the wedge structure is shown in Fig. 9. For calculation purposes the internal side of the FPI is chosen perpendicular to the fiber axis and the external face with a wedge angle ε_w to the direction perpendicular to the fiber axis. The wedge is small enough for us to assume that the reflections from both sides of the FP still overlap and interference occurs. As in the case of a tilt the axial symmetry of the structure is broken. A new distribution of FP thickness appears along the different directions of the divergent beam. In the cylindrical coordinate system centered on the fiber axis in the plane $OxOy$, the new distribution of phase difference will be expressed along each radial direction. The beam footprint on the wedged side of the FPI projected onto the $OxOy$ plane describes an ellipse centered on O', as defined by

$$\frac{(x - x_0)^2}{b^2} + \frac{y^2}{c^2} = 1, \tag{22}$$

with

$$x_0 = -(r_0 + l_0 \tan \theta_d) \frac{\tan \theta_d \tan \varepsilon_w}{1 - \tan^2 \theta_d \tan^2 \varepsilon_w}, \tag{23}$$

$$b = (r_0 + l_0 \tan \theta_d) \frac{1}{1 - \tan^2 \theta_d \tan^2 \varepsilon_w}, \tag{24}$$

$$c = r_0 + l_0 \tan \theta_d, \tag{25}$$

where r_0 is given by

$$r_0 = z_i \tan \theta_{d1} = a + z_0 \tan \theta_{d1}. \tag{26}$$

The distance $r(\alpha)$, similar to the tilt case, can be calculated with Eq. (15). The exact solution is given by

$$r(\alpha) = (r_0 + l_0 \tan \theta_d) \times \frac{-\tan \theta_d \tan \varepsilon_w \cos \alpha + \left[\dfrac{1 - (\tan \theta_d \tan \varepsilon_w \cos \alpha)^2}{1 - \tan^2 \theta_d \tan^2 \varepsilon_w}\right]^{1/2}}{1 - (\tan \theta_d \tan \varepsilon_w \cos \alpha)^2}. \tag{27}$$

For values of angle ε_w below 0.1° and θ_d below 10°, we can safely use the approximation $\tan \varepsilon_w \tan \theta_d \ll 1$ to finally obtain an expression of $r(\alpha)$ independent of angle α:

$$r = r_0 + l_0 \tan \theta_d. \tag{28}$$

This result means that the ellipse described by $r(\alpha)$ nearly coincides with the original circle of the beam footprint in the plane $OxOy$ when there is no wedge. However, because of the wedge angle, the thickness of the FP cavity is no longer constant. It varies along each radial direction α between l_0 and $l_0 - \Delta l(\alpha)$, where $\Delta l(\alpha)$ is given by the relation

$$\Delta l(\alpha) = r \tan \varepsilon_w \cos \alpha. \tag{29}$$

This term directly affects the phase dispersion $\Delta\phi(\alpha)$ that becomes a function of α as well as the distribution of phase differences:

$$\begin{cases} D(\phi_\alpha) = 1 \text{ for } \phi_\alpha \in [\phi_0;\ \phi_0 - \Delta\phi(\alpha)] \\ \quad \text{with } \Delta\phi(\alpha) = \phi_0 \left\{1 - \left[1 - \dfrac{\Delta l(\alpha)}{l_0}\right] \cos \theta_d\right\}. \\ D(\phi_\alpha) = 0 \text{ elsewhere} \end{cases} \tag{30}$$

We obtain the total reflected intensity by integrating the phase differences over angle α between 0 and π, repeating the double integration of Eq. (20).

Because r is a function of z_0, the reflected light intensity is now dependent on the distance separating the fiber from the FPI. In practice this means that the visibility of the fringe is much more sensitive to a wedge when the FPI is moved away from the fiber. However, we are mainly interested in the case in which the FPI is close to the fiber end face.

The visibility versus the average phase dispersion is plotted in Fig. 10 for different values of the wedge angle. Unlike the tilt case, a wedge in the FPI sig-

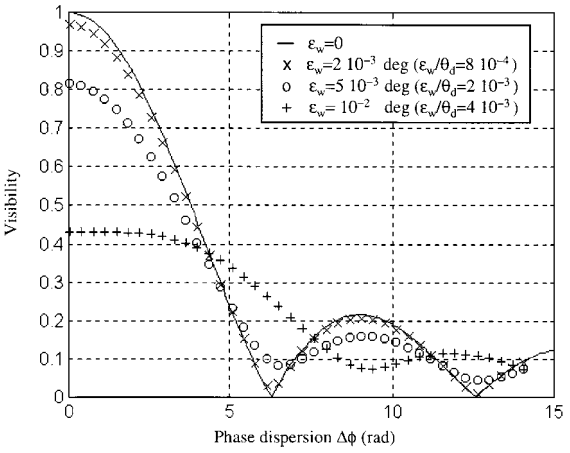

Fig. 10. Visibility versus phase dispersion for different values of the wedge angle ε_w. $R_1 = R_2 = 0.04$, $\theta_{d1} = \theta_d = 4°$, $z_0 = 22$ cm, $n = n_1 = n_2 = 1$.

nificantly affects the visibility for very small phase dispersion. A comparison of Figs. 10 and 7 shows that, under the same experimental condition, wedge angles that are 2 orders of magnitude smaller are enough to begin to start reducing the visibility significantly. The secondary maxima are shifted and smoothed as in the tilt case but they always are accompanied by a reduction of the initial visibility. The experimental data in Fig. 5 show that there is only a very small discrepancy between the theoretical visibility curve for an ideal interferometer and that obtained experimentally for small values of phase dispersion ($\Delta\phi < 5$ rad). Therefore we can attribute the discrepancy for values of phase dispersion close to 2π to the presence of a tilt angle rather than a wedge in the experimental setup.

By using the configuration described in Subsection 4.A, in which a 50-μm-thick cavity is in optical contact with the fiber, we calculate the fringe visibility for increasing values of the wedge angle. The calculation is performed for $z_0 = 0$, $n_1 = n_f = 1.47$, $\theta_{d1} = \theta_d$, and $n_2 = 1.33$, and the results are plotted in Fig. 11 for two different values of the divergence. It clearly shows that a wedge angle above a threshold value of 10^{-2} deg affects the visibility significantly. In terms of the uniformity of cavity thickness, this means that the variations in thickness should not exceed 60 nm over the whole fiber cross section in order to retain maximum visibility.

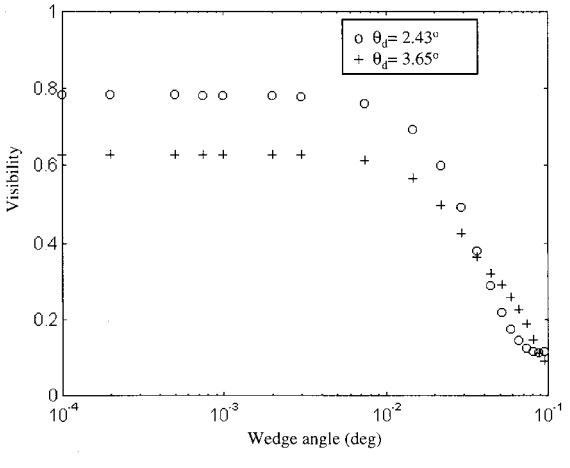

Fig. 11. Visibility versus wedge angle for a 50-μm-thick cavity in optical contact with the fiber tip for two different values of the divergence θ_d ($z_0 = 0$, $n = 1.64$, $n_1 = n_f = 1.47$, $n_2 = 1.33$, $l = 50$ μm, and $\lambda = 850$ nm).

5. Conclusions

A simple analytical model of an ideal multimode FPI has been developed and experimentally validated. This showed that, if significant reductions in fringe visibility that are due to phase dispersion are to be avoided, the divergence of the incident illumination must be minimized. In practice, the use of low-NA (<0.1) optical fibers to illuminate FPI's with thicknesses of less than 100 μm will allow a visibility close to the optimum to be achieved. The model has been extended to describe the effect of imperfections on performance. The effect of a tilt angle between the fiber axis and the FPI is of minimal significance, providing it can be kept below approximately 1° for sensing configurations in which the cavity is in optical contact with the fiber end face: A 1° end angle can be readily achieved with standard fiber end-face preparation techniques such as cleaving or polishing. When the FPI geometry resembles that of a wedge, the thickness across the illuminated region is no longer constant and phase dispersion is modified, resulting in a reduction in visibility. This sets tight limits on the acceptable tolerance for nonuniformities in thickness. For example, for a 50-μm-thick cavity positioned close to a 380-μm fiber core cross section, the thickness tolerance over this area needs to be of the order of several tens of nanometers. It is considered that the models reported in this paper provide a useful tool for the design and optimization of multimode FP sensors.

This research was supported by the British Heart Foundation and the Engineering and Physical Sciences Research Council (U.K.).

References

1. T. Yoshino, K. Kurosawa, K. Itoh, and T. Ose, "Fiber-optic Fabry–Perot interferometer and its sensor applications," IEEE Trans. Microwave Theory Tech. **MTT-30,** 1612–1621 (1982).
2. R. A. Wolthius, G. L. Mitchell, E. Saaski, J. C. Hartl, and M. A. Afromowitz, "Development of medical pressure and temperature sensors employing optical spectrum modulation," IEEE Trans. Biomed. Eng. **38,** 974–981 (1991).
3. A. K. Murphy, M. F. Gunter, A. M. Vengsarker, and R. O. Claus, "Quadrature phase-shifted, extrinsic Fabry–Perot optical fiber sensors," Opt. Lett. **16,** 273–275 (1991).
4. V. Arya, M. J. de Vries, K. A. Murphy, A. Wang, and R. O. Claus, "Exact analysis of the EFPI optical fiber sensor using Kirchhoff's diffraction formalism," Opt. Fiber Technol. **1,** 380–384 (1995).
5. E. R. Cox and B. E. Jones, "Fiber optic colour sensors based on Fabry–Perot interferometry," in *Proceedings of the First International Conference on Optical Fiber Sensors* (Optical Society of America, Washington, D.C., 1983), pp. 122–126.

6. P. C. Beard and T. N. Mills, "A miniature optical fibre ultrasonic hydrophone using a Fabry–Perot polymer film interferometer," Electron. Lett. **33,** 801–803 (1997).
7. A. J. Coleman, E. Draguioti, R. Tiptaf, N. Shotri, and J. E. Saunders, "Acoustic performance and clinical use of a fibre-optic hydrophone," Ultrasound Med. Biol. **24,** 143–151 (1998).
8. P. C. Beard and T. N. Mills, "Extrinsic optical fiber ultrasound sensor with a thin polymer film as a low-finesse Fabry–Perot interferometer," Appl. Opt. **35,** 663–675 (1996).
9. P. C. Beard, F. Pérennès, E. Draguioti, and T. N. Mills, "Optical fiber photoacoustic–photothermal probe," Opt. Lett. **23,** 1235–1237 (1998).
10. T. Liu, D. Brooks, A. Martin, R. A. Badcock, B. Ralph, and G. F. Fernando, "A multimode fibre based extrinsic Fabry–Perot interferometric strain sensor," J. Smart Mater. Structures **6,** 464–469 (1997).
11. V. Arya, M. J. de Vries, M. Athreya, A. Wang, and R. O. Claus, "Analysis of the performance of imperfect fiber endfaces on the performance of extrinsic Fabry–Perot interferometric optical fiber sensors," Opt. Eng. **35,** 2262–2265 (1996).
12. E. Hecht, *Optics*, 2nd ed. (Addison-Wesley, Reading, Mass., 1987), pp. 364–366.
13. J. L. Santos, A. P. Leite, and D. A. Jackson, "Optical fiber sensing with a low-finesse Fabry–Perot cavity," Appl. Opt. **31,** 7361–7366 (1992).